International Journal of Adhesion & Adhesives 44 (2013) 232–236

Contents lists available at SciVerse ScienceDirect

International Journal of Adhesion & Adhesives

journal homepage: www.elsevier.com/locate/ijadhadh

Electrical and mechanical properties of electrically conductive adhesives from epoxy, micro-silver flakes, and nano-hexagonal boron nitride particles after humid and thermal aging

Hui-Wang Cui [a,b,c,*], Dong-Sheng Li [a], Qiong Fan [a], Hua-Xiang Lai [a]

[a] Key State Laboratory for New Displays & System Applications and SMIT Center, College of Automation and Mechanical Engineering, Shanghai University, Shanghai 200072, China
[b] Department of Material and Optoelectronic Science, National Sun Yat-Sen University, Kaohsiung 804-401, Taiwan
[c] Institute of Scientific and Industrial Research, Osaka University, Ibaraki 565-0047, Osaka, Japan

ARTICLE INFO

Article history:
Accepted 19 March 2013
Available online 28 March 2013

Keywords:
Conductive adhesives
Electronics
Mechanical properties of adhesives

ABSTRACT

In this study, we incorporated micro-silver flakes and nano-hexagonal boron nitride (BN) particles into a matrix resin to prepare electrically conductive adhesives (ECAs). The humid and thermal aging results under a constant relative humidity level of 85% at 85 °C revealed that the aged ECAs containing 3 wt% of nano-hexagonal BN particles had high reliability. The contact resistance was low and the shear strength high. Nano-hexagonal BN particles have a good effect on the reliability of ECAs that can be used to improve the properties of ECAs.

© 2013 Elsevier Ltd. All rights reserved.

1. Introduction

As an environment friendly alternative to lead bearing solders, electrically conductive adhesives (ECAs) have many advantages, such as few processing steps to reduce fluxing and cleaning of the components to lower the processing cost, low processing temperatures to enable the use of heat-sensitive and low cost components and substrates, fine pitch interconnection capability, etc. [1–8]. However, compared to the mature soldering technology, ECAs still have some shortcomings—relatively low conductivity, unstable contact resistance, and relatively bad reliability—that limit the application fields to a certain extent [9–13]. In addition, the reliability is very important to the electronic products, which require that the electronic packaging materials have good electrical, mechanical, and thermal properties [14–24]. In humid and thermal surroundings, the electrochemical corrosion at the contact interface caused by the water gain of polymer matrixes, the internal hydrolysis of colloids themselves, the stress concentration caused by the surrounding changes, the delamination between devices, etc., all are likely to increase the electrical resistance and reduce the bonding strength, and thus cause the failure of electronic devices [14–24]. Therefore, the reliability of ECAs in the humid and thermal surroundings has been a hot research focus all the time. In this study, the electrical and mechanical properties of ECAs after a humid and thermal aging were investigated.

In our previous studies, a matrix resin composite of a functional epoxy, a reactive diluent, a silane coupling agent, and a curing agent was fixed, and a formulation of ECAs containing 25 wt% of matrix resin and 75 wt% electrically conductive fillers was optimized. These ECAs were cured completely at 150 °C for 30 min, had a high pyrolysis temperature above 350 °C and a high glass transition temperature at 180 °C [25–28]. In addition, some high performance uni-modal, bi-modal, tri-modal, flexible, and fast curing ECAs were also developed from the matrix resin, micro-silver flakes, micro-silver spheres, nano-silver spheres, and carbon nanotubes [29–34]. In this study, the matrix resin and the formulation described above were still used. We then incorporated micro-silver flakes and nano-hexagonal boron nitride (BN) particles into the matrix resin to prepare ECAs, the electrical and mechanical properties of which we investigated under a constant relative humidity level of 85% at 85 °C (85 °C and 85% RH) for 500 h.

2. Experiment

2.1. Samples

ECAs were a composite of matrix resin, micro-silver flakes, and nano-boron nitride particles. The matrix resin contained a functional epoxy (N, N-diglycidyl-4-glycidyloxyaniline, Sigma-Aldrich, MO, USA) as the main resin, a reactive diluent (2-ethylhexyl glycidyl ether, Sigma-Aldrich, MO, USA), a silane coupling agent

* Corresponding author at: College of Automation and Mechanical Engineering, Key State Laboratory for New Displays & System Applications and SMIT Center, Shanghai University, Shanghai 200072, China. Tel.: +86 2156331599; fax: +86 2156632054.
E-mail address: cuihuiwang@hotmail.com (H.-W. Cui).

0143-7496/$ - see front matter © 2013 Elsevier Ltd. All rights reserved.
http://dx.doi.org/10.1016/j.ijadhadh.2013.03.007

Table 1
Design of ECAs and ECA-BN samples.

	Matrix resin (wt%)	Micro-silver flakes (wt%)	Nano-hexagonal BN (wt%)
ECA	25	75	–
ECA-BN-A	24.5	75	0.5
ECA-BN-B	23.5	75	1.5
ECA-BN-C	22.5	75	2.5
ECA-BN-D	22	75	3
ECA-BN-E	20	75	5

(3-glycidoxypropyltrimethoxysilane, Sigma-Aldrich, MO, USA), and a curing agent (1-cyanoethyl-2-ethyl-4-methylimidazole, Shikoku Chemicals, Chiba, Japan). Their ratios were 75 wt%, 23 wt%, 1 wt%, and 1 wt% respectively in the matrix resin. The size of the micro-silver flakes was 4–8 μm and the thickness was 0.5 μm (Silcoat AgC-A, Fukuda Metal Foil & Powder, Kyoto, Japan). The size of the nano-hexagonal BN particles was less than 100 nm (CWnano, Shanghai, China). As Table 1 shows, the micro-silver flakes were fixed at 75 wt%, the matrix resin at 20–25 wt%, and the nano-hexagonal BN particles at 0–5 wt%. To fabricate these ECAs, the matrix resin was prepared first: the functional epoxy, reactive diluent, silane coupling agent, and curing agent were mixed together using a 78-1 magnetic mixer (Lantian, Hangzhou, China) until they became homogeneous; then the micro-silver flakes and nano-hexagonal BN particles were incorporated into the matrix resin using a MIX500D SLOPE solder cream mixer (Smtech, Shenzhen, China) with a speed of 3000–4000 rpm and a time of 10–20 min. After the fabrication, the obtained ECAs (Table 1, Fig. S1) were stored at −20 °C. For testing, they were taken out to room temperature, thawed for about 30 min, and stirred strongly for about 5–10 min to make sure the fillers were distributed more evenly.

2.2. Characterization

The humid and thermal aging of samples was conducted using a MCU-800 constant temperature and humidity experimental box (Minch Technology, Taiwan) at 85 °C and 85% RH for 500 h. This equipment adopts the surface evaporative humidification and stainless steel cooling-heating systems to control the temperature and humidity. To obtain the contact resistance, the samples were prepared according to Fig. S2(a). A FR-4 printed circuit board (PCB) had a metal coating of Au/Ni/Cu on the lap-joints and the Cu coating contacted with ECAs; the 1206 chip resistor had a surface metal coating of Ag/Ni/Sn and the Sn coating contacted with ECAs (Fig. S2 (b)). After aging at 85 °C and 85% RH, the contact resistance of samples was obtained using a Hewlett & Packard HP-34401A (HP, CA, USA) to measure the voltage (U) and an Agilent E3631A Triple Output DC Power Supply (HP, CA, USA) to measure the supply current (I). Each test point was repeated 50 times. To obtain the shear strength, the samples were prepared according to Fig. S3(a). Another FR-4 PCB substrate (50 mm × 8 mm × 2 mm) with a metal coating of Au/Ni/Cu on the lap-joints was used. The ECAs were printed on the lap-joints using a mask. The thickness of cured ECAs was about 0.1 mm. After aging at 85 °C and 85% RH, the shear strength of samples was obtained using an Instron 5548 Microtester (Instron, MA, USA) at a tensile rate of 5 mm min^{-1} (Fig. S3(b)). Five samples were tested for each value. The shear strength (σ, MPa) was calculated by

$$\sigma = \frac{F}{BD}$$

where σ (MPa) is the shear strength, F (N) is the maximum load, and B (mm) and D (mm) are the length and width of fracture region respectively. The water absorption of samples was obtained at 85 °C and 85% RH. The ECAs were printed onto an aluminum foil using a mask. The thickness of the mask was 0.1 mm and the size of the mask holes was 2 mm × 2 mm. Five samples were tested for each value. The water absorption (φ, %) was calculated by

$$\varphi = \frac{m_t - m_0}{m_0} \times 100$$

where m_0 (g) is the weight of samples before aging and m_t (g) is the weight of samples that absorbed water. The separation and delamination of samples was observed using a PVA TePla SAM400 Quad (QUESTAR, Guangzhou, China).

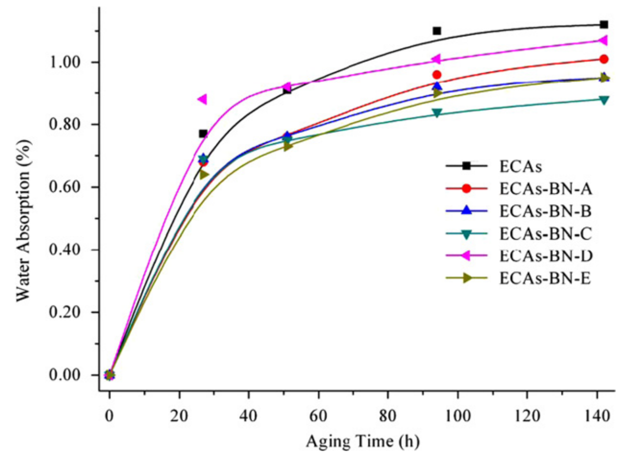

Fig. 1. Water absorption of ECAs and ECA-BN vs aging time.

3. Results and discussion

During the humid and thermal aging, ECAs absorbed water vapor, which gathered on the surface of ECAs firstly, and then penetrated, diffused in ECAs, and saturated eventually, as the aging time increased. There were three factors influencing the water absorption. Firstly, the hydrophilic matrix resin of ECAs increased the water absorption. Secondly, the nano-hexagonal BN particles had a good dispersion in water showing their hydrophilicity [35–38], which increased the water absorption also. Finally, there were voids and gaps in the cured ECAs because of the incorporation of micro-silver flakes, which were helpful for the penetration and diffusion of water vapor in ECAs, while the incorporated nano-hexagonal BN particles filled and occupied some of them to delay and reduce this penetration and diffusion that coincided well with the dual mode sorption theory [39–43]. As Fig. 1 shows, the water absorption increased sharply from 0 h to 40 h, showing that the water vapor penetrated and diffused quickly in ECAs during the initial 40 h [29,44,45]. Thereafter, as the aging time lengthened from 40 h to 130 h, the water vapor continued to penetrate and diffuse in ECAs slowly, leading to saturation eventually.

As described above, the hydrophilic matrix resin, hydrophilic nano-hexagonal BN particles, and the voids and gaps in cured ECAs caused the water absorption mainly. As the nano-hexagonal BN particles increased from 0 wt% (normal ECAs) to 2.5 wt% (ECA-BN-C), the matrix resin decreased and some voids and gaps were filled and occupied, which both combined together to decrease the water absorption; increasing nano-hexagonal BN particles increased the water absorption. However, the decrement had a more significant effect than the increment, so the water absorption decreased from normal ECAs to ECA-BN-C, as shown in Fig. 1. As the nano-hexagonal BN particles increased to 3 wt% (ECA-BN-D), the decreasing matrix resin continued to decrease the water absorption and the

increasing nano-hexagonal BN particles continued to increase the water absorption, while the voids and gaps were filled and occupied completely and hence did not to continue to decrease the water absorption. In other words, the increment was higher than the decrement on the water absorption, so ECA-BN-D had higher values (Fig. 1). Apparently, the filled and occupied voids and gaps did not influence the water absorption any more when the nano-hexagonal BN particles exceeded 3 wt% at ECA-BN-D. When it reached to 5 wt% (ECA-BN-E), more nano-hexagonal BN particles were incorporated into the ECAs to achieve high-density close contacts between/among themselves and the micro-silver flakes, so the contact interfaces with water vapor were reduced to some extent to delay and decrease the absorbing water behaviors. Therefore, the water absorption decreased again for ECA-BN-E. As Fig. 1 shows, the maximum water absorption was obtained in the aged normal ECAs and the minimum value in the aged ECA-BN-C. These water absorptions of all normal ECAs and ECAs-BN were in the range of 0.80–1.10 wt% showing that the nano-hexagonal BN particles did not increase the water absorption, which is a key factor influencing the reliability of ECAs [46–48].

The water vapor increased the stress at the contact interface between ECAs and devices to produce micro-cracks, and then reduced the contact area between them to increase the contact resistance. Moreover, the water vapor also entered the produced micro-cracks to expand them into long or large cracks to increase the contact resistance further. As Fig. 2 shows, the darker color at a and b showed that there were tight, dense contact interfaces between ECAs and devices, and they contacted with each other closely before aging; while those at c and d were lighter showing that there were cracks, separations, and delaminations between ECAs and devices, which had a negative, even bad effect on the electrical and mechanical properties of ECAs.

It can be seen from Fig. 3 that the contact resistance of ECAs seemed to have similar variation trends as that of water absorption. As Fig. 1 shows, the water saturated in ECAs in the initial 130 h of aging time that meant the water absorption, voids, gaps, and cracks all were formed almost completely in this time, and then remained in a stable state beyond this point. Therefore, the contact resistance increased as the aging time lengthened increased sharply from 0 h to 130 h and stabilized slowly and gradually from 130 h to 500 h, showing that the saturated water did not have more negative or bad effect on the contact resistance of ECAs.

It can be also seen from Fig. 3 that the maximum contact resistance was obtained in the aged ECA-BN-C and the minimum value in the aged ECA-BN-D that differed from the water absorption shown in Fig. 1, where the maximum water absorption was in the aged normal ECAs and the minimum value in the aged ECAs-BN-C. Thus, we can predict that besides the water vapor, nano-hexagonal BN particles, voids, gaps, cracks, separations, and delaminations mentioned above, the electrochemical reactions caused by them in the humid and thermal aging also influenced the contact resistance.

In the humid and thermal surroundings, the water vapor penetrated, diffused in ECAs, and entered into the contact interface between ECAs and devices, which provided a good environment for the formation of surface corrosion of metals on the devices. Hence, three items water vapor, the micro-silver flakes, and the surface metals on the devices, formed a micro-electrolytic cell to corrode the surface metal on the devices further. As Fig. 4(c) shows, the contact interface (bonding area) was silver-white before aging while that of aged became black in color, which showed that the electrochemical reaction occurred indeed among the water vapor, the micro-silver flakes, and the surface metals on the devices, However, the incorporated nano-hexagonal BN particles restrained and weakened the electrochemical reaction to a certain extent because they reduced the micro-silver flakes at the contact interface and reduced the contact area between the micro-silver flakes and the surface metals on the devices also. For ECA-BN-D, as described above, 3 wt% of nano-hexagonal BN particles was incorporated into the ECAs to take the place of the matrix resin with a same weight ratio; they filled and occupied all the voids and gaps completely, and there were closer and denser contact interfaces between ECA-BN-D and devices, which restrained and weakened the electrochemical reactions better. Therefore, all these complex factors mentioned above combined together so that the contact resistance and variation trend of ECAs-BN-D were lower, as shown in Fig. 3. For ECAs-BN-E, because too many nano-hexagonal BN particles were incorporated into the ECAs to have high-density close contacts between/among themselves and the micro-silver flakes, which blocked and reduced the electrically conductive channels formed by the micro-silver flakes; therefore, the contact resistance increased again.

Similarly, the mechanical properties of ECAs were also influenced. As Fig. 4(a) shows, the shear strength increased firstly as the nano-hexagonal BN particles increased from 0 wt% (normal ECAs) to 1.5 wt% (ECA-BN-B), and then decreased. The maximum value was obtained at 10.9 MPa for 1.5 wt% (ECA-BN-B). However, after reaching the maximum shear strength, increasing nano-hexagonal BN particles did not continue to improve the shear

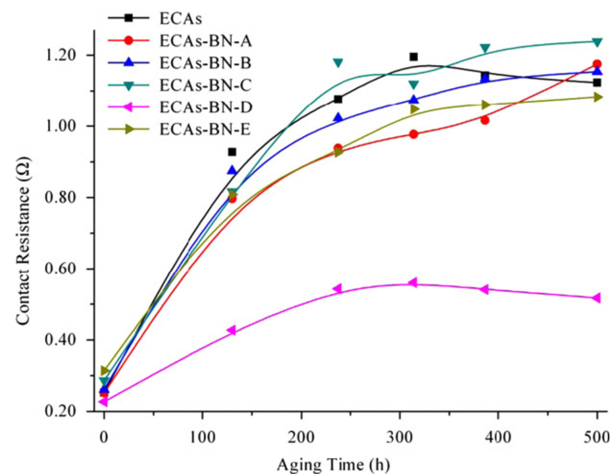

Fig. 3. Contact resistance of ECAs and ECA-BN vs aging time.

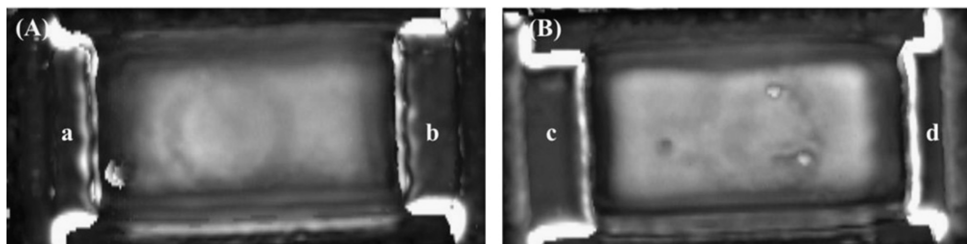

Fig. 2. Contact interface between ECAs and 1206 chip resistor from C-scanning acoustic microscope: (A) before aging and (B) aged, where a, b, c, and d are the contact interfaces between ECAs and devices.

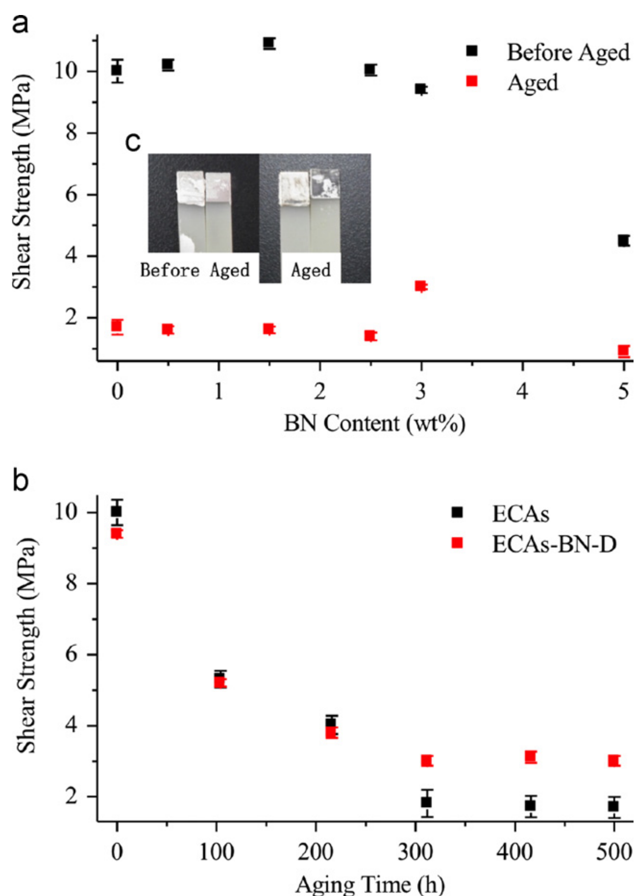

Fig. 4. Shear strength of ECAs and ECA-BN vs (a) nano-hexagonal BN content and (b) aging time, and (c) the fracture morphology of tested samples.

strength and displayed the opposite effect of decreasing it because a few nano-hexagonal BN particles gave a contribution to reinforce the shear strength [49,50] while too many nano-hexagonal BN particles produced more solid-to-solid contacts at the contact interface to reduce the shear strength [51,52]. In addition, the humid and thermal aging also had a negative or bad effect on the shear strength of ECAs as similar to the water absorption and contact resistance. It can be also seen from Fig. 4(c) that the fracture mainly happened on the contact interface (bonding area) between ECAs and devices without damaging the lap-joints. As Fig. 4 shows, the shear strength of aged ECA-BN-D was the maximum. As the aging time lengthened, it decreased slowly (Fig. 4 (b)) resulting from the combined effects of the water vapor, nano-hexagonal BN particles, voids, gaps, cracks, separations, delaminations, and electrochemical reactions. The incorporated nano-hexagonal BN particles filled and occupied all the voids and gaps completely, the contact interfaces (bonding areas) between ECA-BN-D and devices were closer, and denser, the electrochemical reactions were also restrained and weakened, and therefore the decrement of the shear strength was delayed.

4. Conclusions

In this study, micro-silver flakes and nano-hexagonal BN particles were incorporated into a matrix resin to prepare ECAs. During humid and thermal aging, the aged ECA-BN-D containing 3 wt% of nano-hexagonal BN particles had high reliability with a low contact resistance and a high shear strength. Therefore, the nano-hexagonal BN particles have a good effect on the reliability of ECAs that can be used to reinforce the properties of ECAs.

Appendix A. Supporting information

Supplementary data associated with this article can be found in the online version at http://dx.doi.org/10.1016/j.ijadhadh.2013.03.007.

References

[1] Kristiansen H, Liu J. Overview of conductive adhesive interconnection technologies for LCDs. IEEE Trans Components Packag Manuf 1998;21:208–14.
[2] Lu DQ, Wong CP. Development of conductive adhesives for solder replacement. IEEE Trans Components Packag Manuf 2000;23:620–6.
[3] Li Y, Moon KS, Wong CP. Electronics without lead. Science 2005;308:1419–20.
[4] Coughlan FM, Lewis HJ. A study of electrically conductive adhesives as a manufacturing solder alternative. J Electron Mater 2006;35:912–21.
[5] Yim MJ, Paik KW. Review of electrically conductive adhesive technologies for electronic packaging. Electron Mater Lett 2006;2:183–94.
[6] Lewis HJ, Coughlan FM. An overview of the use of electrically conductive adhesives (ECAs) as a solder replacement. J Adhes Sci Technol 2008;2008 (22):801–13.
[7] Yim MJ, Li Y, Moon KS, Paik KW, Wong CP. Review of recent advances in electrically conductive adhesive materials and technologies in electronic packaging. J Adhes Sci Technol 2008;22:1593–630.
[8] Sancaktar E, Bai L. Electrically conductive epoxy adhesives. Polymers 2011;3:427–66.
[9] Kisiel R. Electrically conductive adhesive formulations for SMT applications. J Electron Packag 2002;124:367–70.
[10] Kim JM, Yasuda K, Rito M, Fujimoto K. New electrically conductive adhesives filled with low-melting-point alloy fillers. Mater Trans 2004;45:157–60.
[11] Matienzo LJ, Das RN, Egitto FD. Electrically conductive adhesives for electronic packaging and assembly applications. J Adhes Sci Technol 2008;22:853–69.
[12] Kolbe J. A novel electrically conductive adhesive for use in microelectronics and microsystems by ink jet technology. J Adhes 2009;2009(85):381–94.
[13] Ho LN, Nishikawa H. Surfactant-free synthesis of copper particles for electrically conductive adhesive applications. J Electron Mater 2012;41:2527–32.
[14] Jagt JC. Reliability of electrically conductive adhesive joints for surface mount applications: a summary of the state of the art. IEEE Trans Components Packag Manuf Technol 1998;21:215–25.
[15] Périchaud MG, Delétage JY, Frémont H, Danto Y, Faure C. Reliability evaluation of adhesive bonded SMT components in industrial applications. Microelectron Reliab 2000;40:1227–34.
[16] Kim HK, Shi FG. Electrical reliability of electrically conductive adhesive joints: dependence on curing condition and current density. Microelectron J 2001;32:315–21.
[17] Xiao J, Chung DDL. Electrothermomechanical analysis and its application to studying electrically conductive adhesive joints. J Therm Anal Calorim 2003;74:3–11.
[18] Kim JM, Yasuda K, Yasuda M, Fujimoto K. The effect of reduction capability of resin material on the solder wettability for electrically conductive adhesives (ECAs) assembly. Mater Trans 2004;45:793–8.
[19] Goh CF, Gan ZH, Mhaisalkar SG, Boey FYC, Gusak AM, Teo PS. Modeling of smoothening effect on morphologies of annealed submicron nickel particles used for electrically conductive adhesives. J Appl Phys 2006;100:084302.
[20] Tan FT, Qiao XL, Chen JG, Wang HS. Effects of coupling agents on the properties of epoxy-based electrically conductive adhesives. Int J Adhes Adhes 2006;26:406–13.
[21] Wickham M, Zou L, Hunt C. Measuring the effect of substrate and component finishes on the reliability of isotropic electrically conductive adhesive joints. Solder Surf Mount Technol 2009;21:12–8.
[22] Guan YL, Chen X, Li FQ, Gao H. Study on the curing process and shearing tests of die attachment by Ag–epoxy electrically conductive adhesive. Int J Adhes Adhes 2010;30:80–8.
[23] Ho LN, Wu TF, Nishikawa H, Takemoto T, Miyake K, Fujita M, et al. Electrical reliability of different alloying content on copper alloy fillers in electrically conductive adhesives. J Mater Sci Mater Electron 2011;22:735–40.
[24] Yim BS, Kwon Y, Oh SH, Kim J, Shin YE, Lee SH, et al. Characteristics of solderable electrically conductive adhesives (ECAs) for electronic packaging. Microelectron Reliab 2012;52:1165–73.
[25] Li DS, Cui HW, Chen S, Fan Q, Yuan ZC, Ye LL, et al. A highly conductive bimodal isotropic conductive adhesive and its reliability. ECS Trans 2011;34:583–8.
[26] Du WH, Cui HW, Chen S, Yuan ZC, Ye LL, Liu J. Study on the reliability of fast curing isotropic conductive adhesive. ECS Trans 2011;34:805–10.
[27] Fan Q, Cui HW, Fu CE, Li DS, Tang X, Yuan ZC, et al. The effect of functionalized silver on rheological and electrical properties of conductive adhesives. ECS Trans 2011;34:811–6.
[28] Cui HW, Fan Q, Li DS, Tang X. Formulation and characterization of electrically conductive adhesives for electronic package. J Adhes 2013;89:19–36.
[29] Cui HW, Li DS, Fan Q. Reliability of flexible electrically conductive adhesives. Polym Adv Technol 2013;24:114–7.
[30] Cui HW, Li DS, Fan Q. Using nano-hexagonal boron nitride particles and nano cubic silicon carbide particles to improve the thermal conductivity of electrically conductive adhesives. Electron Mater Lett 2013;9:1–5.

[31] Cui HW, Kowalczyk A, Li DS, Fan Q. High performance electrically conductive adhesives from functional epoxy, micron silver flakes, micron silver spheres and acidified single wall carbon nanotube for electronic package. Int J Adhes Adhes 2013. http://dx.doi.org/10.1016/j.ijadhadh.2013.03.004.

[32] Cui HW, Fan Q, Li DS. Novel flexible electrically conductive adhesives from functional epoxy, flexibilizers, micro silver flakes and nano silver spheres for electronic package. Polym Int 2013 dpi 10.1002/pi.4461.

[33] Cui HW, Du WH. Novel fast curing electrically conductive adhesives from a functional epoxy and micro silver flakes: preparation, characterization, and humid–thermal aging. J Adhes 2013. http://dx.doi.org/10.1080/00218464.2012.757696.

[34] Cui HW, Li DS, Fan Q. Using a functional epoxy, micron silver flakes, nano silver spheres, and treated single-wall carbon nanotubes to prepare high performance electrically conductive adhesives. Electron Mater Lett 2013. http://dx.doi.org/10.1007/s13391-013-2243-y.

[35] Lin Y, Williams TV, Connell JW. Soluble, exfoliated hexagonal boron nitride nanosheets. J Phys Chem Lett 2010;1:277–83.

[36] Lee CH, Zhang DY, Yap YK. Functionalization, dispersion, and cutting of boron nitride nanotubes in water. J Phys Chem C 2012;116:1798–804.

[37] Nazarov AS, Demin VN, Grayfer ED, Bulavchenko AI, Arymbaeva AT, Shin HJ, et al. Functionalization and dispersion of hexagonal boron nitride (h-BN) nanosheets treated with inorganic reagents. Chem-Asian J 2012;7:554–60.

[38] Li L, Li LH, Ramakrishnan S, Dai XJJ, Nicholas K, Chen Y, et al. Controlling wettability of boron nitride nanotube films and improved cell proliferation. J Phys Chem C 2012;116:18334–9.

[39] Huh JK, Song DI, Jeon YW. Sorption of phenol and alkylphenols from aqueous solution onto organically modified montmorillonite and applications of dual-mode sorption model. Sep Sci Technol 1999;35:243–59.

[40] Ramani R, Ranganathaiah C. Free-volume microprobe study of iodine diffusion in polymers. Polym Int 2001;50:237–48.

[41] Feng HD. Modeling of vapor sorption in glassy polymers using a new dual mode sorption model based on multilayer sorption theory. Polymer 2007;48:2988–3002.

[42] Garrido L, Lopez-Gonzalez M, Saiz E, Riande E. Molecular basis of carbon dioxide transport in polycarbonate membranes. J Phys Chem B 2008;112:4253–60.

[43] Wang L, Corriou JP, Castel C, Favre E. Transport of gases in glassy polymers under transient conditions: limit-behavior investigations of dual-mode sorption theory. Ind Eng Chem Res 2013;52:1089–101.

[44] Cui HW, Li DS, Fan Q. Adhesion of a novel flexible epoxy molding compound and its molecular dynamics simulation. Int J Adhes Adhes 2012;35:50–4.

[45] Cui HW, Li DS, Fan Q. Preparation and characterization of a novel epoxy molding compound with low storage modulus at high temperature and low glass-transition temperature. J Electron Mater 2012;41:2599–605.

[46] Xu SY, Dillard DA, Dillard JG. Environmental aging effects on the durability of electrically conductive adhesive joints. Int J Adhes Adhes 2003;23:235–50.

[47] Xu SY, Dillard DA. Environmental aging effects on thermal and mechanical properties of electrically conductive adhesives. J Adhes 2003;79:699–703.

[48] Zhu XY, Liu YL, Long JM, Liu XL. Electrochemical migration behavior of Ag-plated Cu-filled electrically conductive adhesives. Rare Metal 2012;31:64–70.

[49] Kemaloglu S, Ozkoc G, Aytac A. Properties of thermally conductive micro and nano size boron nitride reinforced silicon rubber composites. Thermochim Acta 2010;499:40–7.

[50] Zhang HA, Gu SY, Yi JY. Fabrication and properties of Ti(C, N) based cermets reinforced by nano-CBN particles. Ceram Int 2012;38:4587–91.

[51] Zhang ZY, Zhao P, Xiao GZ. The fabrication of polymer microfluidic devices using a solid-to-solid interfacial polyaddition. Polymer 2009;50:5358–61.

[52] Choi J, Lee JI, Eun Y, Kim MO, Kim J. Aligned carbon nanotube arrays for degradation-resistant, intimate contact in micromechanical devices. Adv Mater 2011;23:2231–6.